Available online at www.sciencedirect.com
SCIENCE DIRECT
Journal of Catalysis 241 (2006) 426–434
JOURNAL OF CATALYSIS
www.elsevier.com/locate/jcat

Dehydroisomerization of butane into isobutene on Pt–Sn intermetallic compounds supported on H-SAPO-11

Takayuki Komatsu *, Hirokazu Ikenaga

Department of Chemistry, Tokyo Institute of Technology, 2-12-1-E1-10 Ookayama, Meguro-ku, Tokyo 152-8550, Japan

Received 14 March 2006; revised 17 May 2006; accepted 20 May 2006

Available online 21 June 2006

Abstract

The dehydroisomerization of butane to form isobutene was carried out on Pt-based bimetallic catalysts supported on zeolite. Among various zeolites, Si-rich H-SAPO-11 was most appropriate for obtaining high selectivity to isobutene at higher butane conversions. The acid sites of Si-rich H-SAPO-11 were characterized by ammonia adsorption, ^{29}Si MAS NMR, and the cracking of cumene. The addition of second elements, such as Sn, Pb, Zn and In, onto Pt/H-SAPO-11 retarded the hydrogenolysis activity of Pt, resulting in decreased methane selectivity. Among the second elements, tin was the most effective additive for obtaining higher isobutene selectivity. The formation of Pt–Sn intermetallic compounds, Pt_3Sn, PtSn, and $PtSn_2$, was revealed by XRD. The surface of Pt–Sn bimetallic particles was characterized through the dispersion of Pt and IR spectra of adsorbed CO. The formation of surface intermetallic compounds is proposed to retard hydrogenolysis by the ensemble effect.

Keywords: Dehydroisomerization; Butane; Isobutene; Intermetallic compound; Platinum; Tin; Silicoaluminophosphate; SAPO-11; Ensemble effect

1. Introduction

Isobutene is one of the key intermediates in the petrochemical industry for the production of methyl methacrylate, polybutene, etc. An FCC process has supplied isobutene as a part of C_4 fractions. An increasing demand for isobutene has stimulated the development of a new route to obtain isobutene from butane. This process is composed of two-step reactions; the isomerization of butane into isobutane and subsequent dehydrogenation of isobutane or the dehydrogenation of butane into 1- and 2-butenes and subsequent isomerization into isobutene. Recently, some researches on the one-step formation of isobutene from butane through the dehydroisomerization using bifunctional catalysts have been reported. Platinum supported on zeolite is widely studied, such as Pt/ZSM-5 [1–3], Pt/MFI-ferrisilicate [4], and Pt/MCM-22 [5].

Because the dehydrogenation of alkane requires high temperatures, the dehydroisomerization of butane was carried out usually at high temperatures around 800 K. The strong Brønsted acid sites on zeolites often catalyze the undesirable cracking, hydride transfer, aromatization, and coke formation as well as isomerization at high temperatures. Therefore, molecular sieves with weaker acid sites have been applied as the isomerization catalyst combined with metal catalysts. Wei et al. [6] studied the catalytic properties of Pd supported on silicoaluminophosphate (SAPO) with AEL, AFI, and CHA framework types. They reported that Pd/SAPO-5 and Pd/SAPO-34 were not effective catalysts because of the insufficient acid strength and too small pore diameters, respectively, and that Pd/SAPO-11 was the best catalyst for the formation of isobutene. They further studied the effect of Si content on the catalytic performance of Pd/SAPO-11 and found that the increased Si content resulted in the increased butane conversion and decreased isobutene selectivity [7]. Vieira et al. [8] studied the effect of Mn on the catalytic properties of Pt/$AlPO_4$-11. When Mn was introduced into the framework of $AlPO_4$-11 to form MnAPO-11, the resultant Brønsted acid sites effectively catalyzed the isomerization, whereas Pt on Mn-impregnated $AlPO_4$-11 was not effective like Pt/$AlPO_4$-11 because of their insufficient acidity. On the active Pt/MnAPO-11, a part of Mn was dispersed as extra-framework species and located on Pt particles to reduce the undesirable hydrogenolysis catalyzed by Pt through the ensemble effect [9].

* Corresponding author. Fax: +81 3 5734 2758.
E-mail address: komatsu@chem.titech.ac.jp (T. Komatsu).

0021-9517/$ – see front matter
doi:10.1016/j.jcat.2006.05.018

To increase the selectivity to isobutene, the hydrogenolysis catalyzed by metal particles must be suppressed. In the case of alkane dehydrogenation, the addition of tin into Pt-catalysts has been reported to be effective in suppressing the hydrogenolysis by Pt particles to increase alkene selectivity [10–13]. The effect of tin in such Pt–Sn bimetallic catalysts would result from the ensemble effect [10,11,14] or a significant ligand effect [15]. For the dehydroisomerization of butane, copper was impregnated on Pt/H-MCM-22, demonstrating that copper suppressed hydrogenolysis by reducing the size of the Pt ensembles at the surface of Pt particles [16]. The hydrogenolysis activity of Pt particles in Pt/H-Y was retarded by co-impregnation of tin [17]. The IR spectra of adsorbed CO indicated that tin apparently was dispersed onto Pt to reduce the large ensemble of Pt active for the hydrogenolysis. In these reports, the state of the second element (Cu or Sn) was not clearly determined, however.

We have studied on the catalytic properties of intermetallic compounds, such as CoGe [18], Pt_3Ge [19], Ni_3Sn and Ni_3Sn_2 [20], and $TiPt_3$ [21]. The combination of a transition metal and a typical element resulted in lower activity than the parent transition metal for H_2–D_2 equilibration [18–20] and hydrogenation of acetylene [18,20] and 1,3-butadiene [19], whereas the combination yielded the highly selective catalyst for the partial hydrogenation of acetylene [18,20] and 1,3-butadiene [19]. On the other hand, the compound between two transition metals, $TiPt_3$, showed much higher activity than Pt for the hydrogenation of ethylene [21]. Recently, we prepared the fine particles of intermetallic compounds by supporting them on the surface of silica. The formation of Ni_3Sn particles on SiO_2 was identified by XRD, XPS [22], TPR, IR, and XANES techniques [23]. The resultant Ni_3Sn/SiO_2 had high selectivity to benzene in the dehydrogenation of cyclohexane as in the case of unsupported Ni_3Sn, whereas the decreased particle size enhanced the activity per gram of Ni_3Sn by a factor of 1000 [22]. $RuTi/SiO_2$ was found to be selective for the formation of higher hydrocarbons in FT synthesis compared with Ru/SiO_2, probably because of the weak hydrogenation activity of RuTi in transforming CH_x intermediates into methane [24]. Pt_3Ge/H-ZSM-5 showed higher selectivity to aromatic hydrocarbons in the aromatization of butane through the suppression of the hydrogenolysis by Pt [25]. Clearly, the intermetallic compounds have unique catalytic properties in the reactions of hydrogenation and dehydrogenation.

In this study, we prepared fine particles of Pt–Sn intermetallic compounds on zeolites for the catalyst in the dehydroisomerization of butane into isobutene. The purposes of this study are to clarify the catalytic properties of Pt–Sn intermetallic compounds in the reaction of butane and to obtain the selective catalyst for the formation of isobutene by using acidic silicoaluminophosphate with weak acidity as the isomerization catalyst.

2. Experimental

2.1. Catalyst preparation

Zeolites were prepared by the usual hydrothermal synthesis for ZSM-5 (Si/Al = 84), ferrierite (12), MFI-ferrisilicate (Si/Fe = 42), and SAPO-5 (Si/(Si + Al + P) = 0.018). SAPO-11 with varying Si content was also prepared hydrothermally using aluminum hydroxide (Cataloid AP-1, 71 wt% Al_2O_3, Catalysts and Chemicals Ind.), phosphoric acid, silica (NIPSIL VN3, Nippon Silica Ind.), and di-*n*-propylamine (Kanto Kagaku) as an SDA. SDA was removed by calcination in flowing air at 873 K for 15 h. USY zeolite of Si/Al = 7.4 was supplied from Catalysts and Chemicals Ind. All of the zeolites were transformed into H form through ion exchange with 0.1 M aqueous solution of ammonium nitrate at 343 K and a subsequent calcination in air at 773 K for 5 h.

Platinum was supported on zeolites with 1 wt% loading by a usual impregnation method with an aqueous solution of $Pt(NH_3)_4(CH_3COO)_2$. After drying at 403 K overnight, the sample was calcined in air at 573 K for 2 h, at 623 K for 3 h, and at 723 K for 4 h. Pt–M/H-SAPO-11 (M = Sn, Pb, Zn, and In) bimetallic catalysts were prepared by a co-impregnation method. $Sn(CH_3COO)_2$, $Pb(CH_3COO)_2$, $Zn(CH_3COO)_2$, or $In(NO_3)_3$ was dissolved in an acetic acid solution of $Pt(NH_3)_4(CH_3COO)_2$, and H-SAPO-11 was impregnated with the solution to have a Pt loading of 1 wt% and a Pt/M atomic ratio of 1.5. The drying and calcination were carried out similarly to that for Pt/zeolite. Pt–Sn/H-SAPO-11 with varying Sn content was prepared by successive impregnation on Pt/H-SAPO-11 prepared by the above method. A specific amount of $Sn(CH_3COO)_2$ was dissolved in an acetic acid solution. Pt/H-SAPO-11 was put into the solution and dried and calcined under the same conditions as those for Pt/zeolites. The resultant catalyst is expressed as Pt–Sn(*n*)/H-SAPO-11, where *n* represents the Pt/Sn atomic ratio.

2.2. Characterization

The crystal structure of synthesized zeolites and supported metal particles was examined by powder X-ray diffraction (Rigaku, RINT2400). Composition of zeolites was measured by ICP (Rigaku, JY38) after dissolving the zeolites with HF solution or with alkali fusion in the case of SAPO. The amount of adsorbed ammonia was measured by a microbalance. A known amount of sample was put in a quartz basket hanging under a quartz spring. After the sample was evacuated at 773 K for 1 h, ammonia (13 kPa) was introduced at 298 K for 0.5 h. The sample was evacuated at 423 K for 0.5 h, and the weight of the sample was recorded. After the evacuation at 773 K for 1 h, the sample weight was again recorded. The amount of acid sites was obtained from the difference between the sample weights before and after the evacuation at 773 K. ^{29}Si MAS NMR spectra were recorded on a Bruker Avance 400 spectrometer at 79.50 MHz. A total of 2000 scans were accumulated to obtain a satisfactory signal-to-noise ratio, with TMS used as a chemical shift reference.

IR spectra of adsorbed CO were measured with a JASCO FT/IR-430 in transmission mode. A self-supporting wafer (ca. 10 mg cm^{-2}) of Pt/H-SAPO-11 or Pt–Sn/H-SAPO-11 was placed into a quartz cell with CaF_2 windows. After reduction in flowing hydrogen at 873 K for 1 h and evacuation at 773 K for 0.5 h, the sample was cooled in vacuo to 298 K. CO (5 kPa)

was introduced for 5 min, and a spectrum was recorded after evacuation at 298 K for 10 min. Spectra were further obtained after evacuation at elevated temperatures for 10 min.

2.3. Catalytic reaction

Dehydroisomerization of butane into isobutene was carried out with a continuous-flow reaction system under atmospheric pressure. A specific amount (0.05–1.5 g) of catalyst was placed in a quartz tubular reactor (17 mm i.d.). Before the catalytic run, the catalyst was reduced in flowing hydrogen at 873 K for 1 h. The reaction was started at 873 K by supplying a reactant gas with molar ratio of $C_4H_{10}/H_2/He = 1/2/5$ and a total flow rate of 40–120 mL min^{-1}. Gaseous products were analyzed using an FID gas chromatograph (Shimadzu, GC-14B) with a column of PLOT Fused Silica coating Al_2O_3/KCl (Varian, 50 m × 0.25 mm i.d.). The yield and selectivity of each product were calculated based on the carbon number of converted butane and expressed in C%.

Conversion of cumene was carried out with the same reaction system as described above. The catalyst (0.10 g) was pretreated with flowing helium at 773 K for 1 h. Cumene (0.10 mmol min^{-1}) was introduced at 673 K with 20 mL min^{-1} of helium carrier. Products were collected in a cold trap at 273 K and analyzed with an FID gas chromatograph (Shimadzu, GC-14B) with a column of PETROCOL DH 100 (Supelco, 100 m × 0.25 mm i.d.). Dehydrogenation of cyclohexane was carried out in a similar manner. The catalyst (0.10 g) was pretreated with flowing hydrogen at 873 K for 1 h. Cyclohexane (0.10 mmol min^{-1}) was introduced at 773 K with 15 mL min^{-1} of hydrogen carrier.

3. Results and discussion

3.1. Butane dehydroisomerization on Pt/zeolite catalysts

The dehydroisomerization of butane into isobutene was carried out on Pt supported on various zeolites to determine the effect of zeolite acidity and pore structure on the selective formation of isobutene. Fig. 1 shows the relation between the selectivity to isobutene and conversion of butane obtained with various amounts of catalyst and flow rates of reactant. Data were taken at 30–150 min on stream, where the conversion decreased continuously with time on stream. The deactivation was fast on Pt/H-USY, probably because of the coke formation and oligomerization inside the supercages. The isobutene formation proceeds successively first into butene isomers and then into isobutene. In addition, side reactions (e.g., cracking, dimerization [oligomerization], aromatization, hydrogenolysis) will affect the selectivity. In fact, methane, ethane, ethylene, propane, propylene, 1- and 2-butene, 1,3-butadiene, isobutane, and higher hydrocarbons (C_{5+}) containing mainly pentene, benzene, toluene, and xylene were obtained as byproducts. Therefore, the isobutene selectivity of different catalysts should be compared at the comparable conversion. As shown in Fig. 1, at low conversion (around 30%), Pt/H-ZSM-5 was most selective for the isobutene formation; however, its selectivity decreased with increasing conversion, whereas the selectivity of Pt/H-SAPO-11 [Si/(Si + Al + P) = 0.11, (B) in Table 2] and Pt/H-MFI-ferrisilicate increased with conversion and reached their maxima at ca. 70 and 80%, respectively. Product distribution on Pt/H-ZSM-5, Pt/H-ferrisilicate, and Pt/H-SAPO-11 at around 75% conversion is shown in Table 1. Pt/H-ZSM-5 gave significant amounts of C_1–C_3 and C_{5+} aromatics, probably because its strong acid sites accelerated the side reactions. Pt/H-ferrisilicate gave a large amount of 1- and 2-butenes. The acid sites would be too weak to catalyze the isomerization. From Fig. 1, except for H-ferrierite, zeolites with pore openings of 10-membered rings seem to be effective for isobutene formation. This result is similar to that for the isomerization of 1-butene into isobutene [26]. We conclude that H-SAPO-11 is the best zeolite with Pt for the dehydroisomerization of butane.

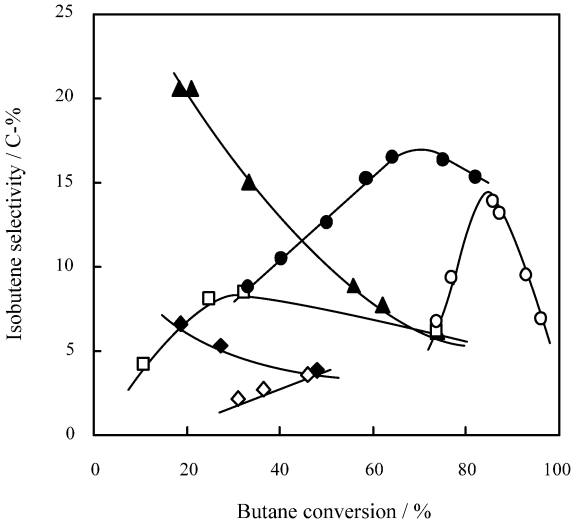

Fig. 1. Isobutene selectivity in the dehydroisomerization of butane on Pt supported on H-ZSM-5 (▲), H-SAPO-11 (●), H-ferrisilicate (○), H-USY (□), H-ferrierite (◆) and H-SAPO-5 (◇).

Table 1
Activity and selectivity of Pt/zeolite catalysts

Catalyst	Conversion (%)	Selectivity (C%)					
		C_1[a]	C_2[b]	C_3[c]	Isobutene	Other C_4[d]	C_{5+}[e]
Pt/H-ZSM-5	73.8	11.9	21.0	27.6	6.2	12.3	18.3
Pt/H-ferrisilicate	73.9	2.7	3.3	7.5	6.7	79.6	0.2
Pt/H-SAPO-11	75.0	7.6	11.7	12.6	16.3	48.1	3.7

[a] Methane.
[b] Ethane and ethylene.
[c] Propane and propylene.
[d] Isobutane, 1- and 2-butene and 1,3-butadiene.
[e] Mainly composed of pentene, benzene, toluene and xylene.

We discuss the side reactions using the hydrogenolysis index (α_{hyd}) in light of the reaction path proposed by Pirngruber et al. [1]. As shown in Scheme 1, methane is formed mainly through initial hydrogenolysis (i), secondary hydrogenolysis (ii), initial cracking of butane (iii), and secondary cracking of octene (iv). Hydrogenolysis (i) provides a CH_4/C_3H_8 molar ratio of 1, and hydrogenolysis (ii) raises the ratio. The cracking (iii) provides a CH_4/C_3H_6 molar ratio of 1, and cracking (iv) reduces the ratio.

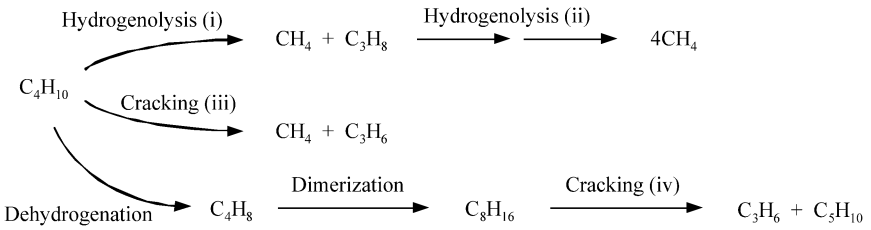

Scheme 1. Hydrogenolysis and cracking from butane.

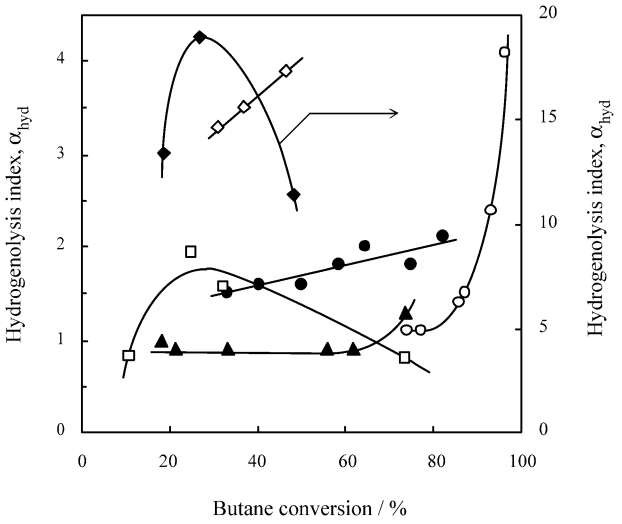

Fig. 2. Hydrogenolysis index of Pt/zeolite catalysts. H-ZSM-5 (▲), H-SAPO-11 (●), H-ferrisilicate (○), H-USY (□), H-ferrierite (◆) and H-SAPO-5 (◇).

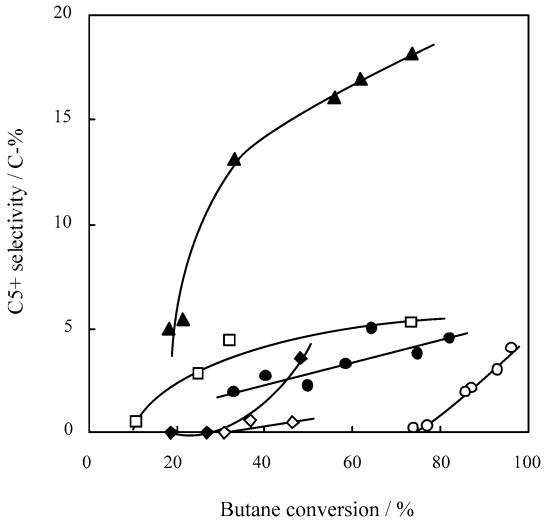

Fig. 3. Selectivity to C_{5+} hydrocarbons on Pt/zeolite catalysts. H-ZSM-5 (▲), H-SAPO-11 (●), H-ferrisilicate (○), H-USY (□), H-ferrierite (◆) and H-SAPO-5 (◇).

We propose the hydrogenolysis index, α_{hyd}, as follows:

$$\alpha_{hyd} = \frac{CH_4 \text{ selectivity (C\%)}}{(C_3H_8 + C_3H_6) \text{ selectivity (C\%)}} \times 3.$$

The catalyst with hydrogenolysis activity dominating cracking activity will give an $\alpha_{hyd} > 1$, whereas that with stronger cracking activity will give a $\alpha_{hyd} < 1$. Fig. 2 shows the α_{hyd} values of the Pt-supported zeolites. Pt/H-ferrierite gave especially high α_{hyd}, indicating its strong hydrogenolysis activity. Pt/H-SAPO-5 also gave $\alpha_{hyd} > 1$, probably because the cracking activity is very low on its weak acid sites. In contrast, Pt/H-ZSM-5 gave low α_{hyd} in a wide range of conversion, indicating high cracking activity on its strong acid sites. The α_{hyd} value of Pt/H-ferrisilicate increased steeply with increasing conversion. Pt/H-SAPO-11 showed medium value (1.5–2) of α_{hyd}. The activity of metal and acid sites would be balanced appropriately on Pt/H-SAPO-11 to avoid the dominating contribution of a specific side reaction. Fig. 3 shows the C_{5+} selectivity of the same series of catalysts. Pt/H-ZSM-5 exhibited the highest C_{5+} selectivity because of its strong activity for aromatization. This aromatization resulted in the decrease in isobutene selectivity with conversion shown in Fig. 1. Other zeolites did not have high selectivity to aromatization.

The selectivity for isomerization was estimated by the percentage of isobutene selectivity to the sum of butene selectivities, as shown in Fig. 4. Under our reaction conditions, this selectivity is suppressed to <40% by the thermodynamic equilibrium. Pt/H-ZSM-5 with strong acid sites showed a high ratio

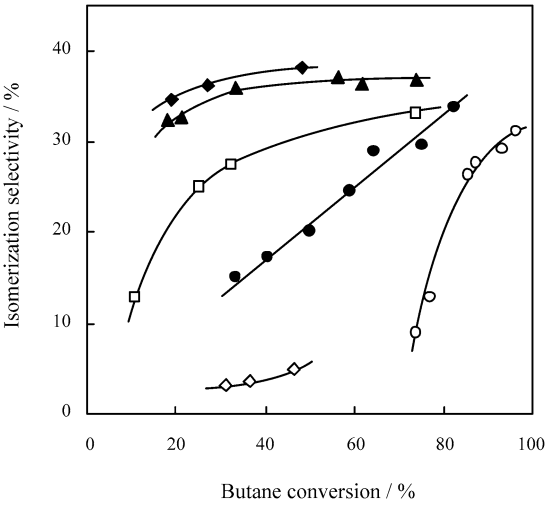

Fig. 4. Selectivity for the isomerization of butenes on Pt/zeolite catalysts. H-ZSM-5 (▲), H-SAPO-11 (●), H-ferrisilicate (○), H-USY (□), H-ferrierite (◆) and H-SAPO-5 (◇).

close to equilibrium even at low conversions. The acid sites would be too strong for the isomerization, and the side reactions (e.g., cracking and aromatization) would readily occur. Pt/H-ferrierite also showed high isomerization selectivity. The acid sites might be strong even though the hydrogenolysis index was high (Fig. 2). Pt/ferrierite was reported to have highly dispersed Pt. As a result, Pt/H-ferrierite showed higher selectiv-

ity to hydrogenolysis than Pt/H-ZSM-5 and Pt/ZSM-22, even though the contribution of cracking was also higher in Pt/H-ferrierite [3]. Although we did not measure the dispersion of Pt on ferrierite, the high dispersion of Pt might cause the high α_{hyd}. Pt/H-SAPO-5 and Pt/H-ferrisilicate gave low isomerization selectivity. Their acid strength would not be sufficient for the isomerization of butene. The acid strength of H-ferrisilicate seems to be comparable to or stronger than that of H-SAPO-11. Our H-ferrisilicate might have a significant number of extra-framework iron atoms and a fewer number of Brønsted acid sites. As shown in Fig. 4, the isomerization selectivity of Pt/H-SAPO-11 increased with increasing conversion, to >30% at higher conversions. The intermediate isomerization selectivity of H-SAPO-11 was appropriate for the selective formation of isobutene; however, the maximum selectivity of Pt/H-SAPO-11 was slightly lower than the equilibrium value. Some enhancement in acidity will increase the isobutene selectivity of Pt/H-SAPO-11.

3.2. Pt supported on H-SAPO-11 with varying Si content

We prepared H-SAPO-11 with varying Si content to clarify the effect of acidity in H-SAPO-11 on isobutene formation. Table 2 shows the Si content, surface area, and number of acid sites for each H-SAPO-11, where H-SAPO-11(B) is the support described in Figs. 1–4. XRD revealed the presence of AEL structure for all H-SAPO-11. The specific surface areas indicated that all the samples have comparable crystallinity. The amount of acid sites, measured by ammonia adsorption, increased with increasing Si content, except for H-SAPO-11(E). The Si content reached saturation around $Si/(Si+Al+P) = 0.2$ in our synthesis procedure. Pt was loaded on H-SAPO-11 (B), (C), (D), and (E), and the resulting catalysts were tested for the butane dehydroisomerization. Fig. 5 shows the isobutene selectivity of Pt/H-SAPO-11 with varying Si content. As expected, increased Si content resulted in increased isobutene selectivity. For Pt/H-SAPO-11 (D) and (E), which had the greatest number of acid sites, isobutene selectivity exceeded 20 C%. Wei et al. [7] studied the effect of Si content on the catalytic properties of Pd/H-SAPO-11 for the dehydroisomerization of butane and found that conversion increased but isobutene selectivity decreased with increasing Si content. Fig. 6 shows the isomerization selectivity obtained in a manner similar to that for Fig. 4. The isomerization selectivity of Pt/H-SAPO-11 (D) and (E) was higher than that of Pt/H-SAPO-11 (B) and (C). The increased number of acid sites was shown to enhance the isomerization of butene on Pt/H-SAPO-11; however, both acid strength and acid amount are altered by changing the Si content in silicoaluminophosphate [27]. The extensive substitution of Si in SAPO forms the Si-rich island containing some Al atoms, called the aluminosilicate region [28]. For H-SAPO-5, the acid strength of protons associated with Al atoms in this aluminosilicate region was reported to be stronger than that of protons associated with Si atoms in the usual SAPO region in the isomerization of *o*-xylene [29]. We measured the catalytic activity of H-SAPO-11 for the cracking of cumene to clarify the acid strength of H-SAPO-11 with varying Si content. Fig. 7 shows the cumene conversion as a function of the number of acid sites. H-SAPO-11(A) with an acid amount of 0.18 mmol g^{-1} did not show significant activity; it did not have sufficient strong acid sites for the cracking of cumene. The conversion steeply increased

Table 2
Properties of SAPO-11 with various Si contents

Catalyst	Si/(Si + Al + P)[a]	Specific surface area[b] ($m^2\ g^{-1}$)	Amount of acid sites[c] (mmol g^{-1})
H-SAPO-11(A)	0.06	214	0.18
H-SAPO-11(B)	0.11	221	0.31
H-SAPO-11(C)	0.17	225	0.35
H-SAPO-11(D)	0.19	225	0.41
H-SAPO-11(E)	0.26	247	0.39

[a] Atomic ratio.
[b] Obtained from Langmuir equation.
[c] Obtained from ammonia adsorption.

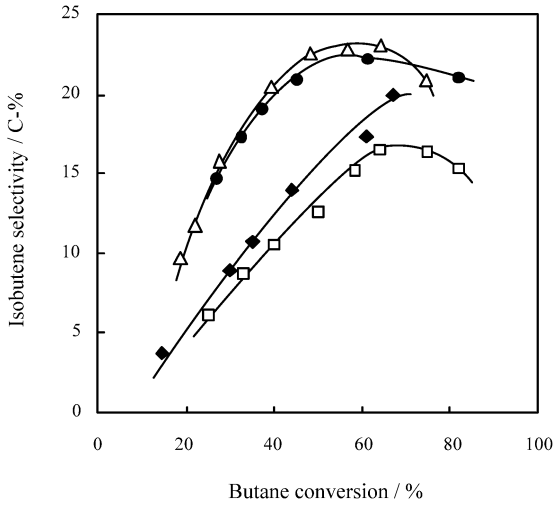

Fig. 5. Isobutene selectivity in the dehydroisomerization of butane on Pt/H-SAPO-11 with various Si contents. Pt/H-SAPO-11(B) (□), Pt/H-SAPO-11(C) (◆), Pt/H-SAPO-11(D) (●) and Pt/H-SAPO-11(E) (△).

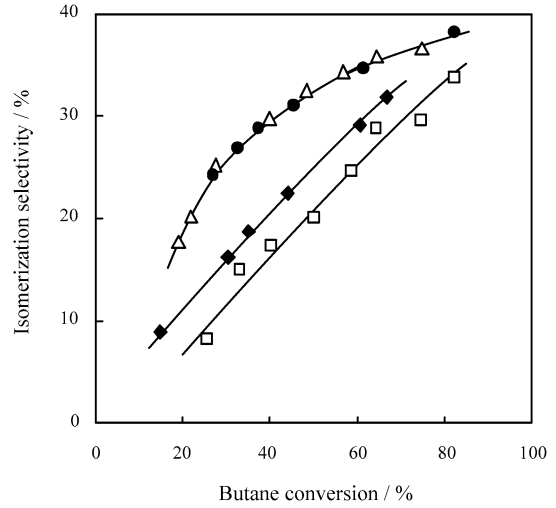

Fig. 6. Selectivity for the isomerization of butenes on Pt/H-SAPO-11. Pt/H-SAPO-11(B) (□), Pt/H-SAPO-11(C) (◆), Pt/H-SAPO-11(D) (●) and Pt/H-SAPO-11(E) (△).

when the acidity exceeded 0.3 mmol g^{-1}, indicating the appearance of strong acid sites. It is clear that the acid strength per acid site in Si-rich H-SAPO-11 is much stronger than that in H-SAPO-11 with low Si content.

We measured ^{29}Si MAS NMR spectra to investigate the formation of a Si-rich region in H-SAPO-11 (Fig. 8). The peaks ascribed to Si(4Al), Si*(4Al), Si(3Al), Si(2Al), Si(1Al), and Si(0Al) are expected to appear at −86, −91, −97, −102, −107, and −110 ppm, respectively [30]. Si*(4Al) represents Si atoms with four Al neighbors in the usual SAPO region, whereas Si(4Al) represents those in the aluminosilicate region. H-SAPO-11(B) with low Si content showed peaks mainly around −90 ppm, indicating the dominant presence of the usual SAPO region. The contribution of peaks at >100 ppm increased with Si content. H-SAPO-11 (D) and (E) showed a strong peak centered at −110 ppm, indicating that most of Si atoms were present in Si-rich islands, such as the silica or aluminosilicate region. The results shown in Figs. 7 and 8 indicate that the acid sites in or around the aluminosilicate region in Si-rich H-SAPO-11 were much stronger than those in the SAPO region. We can conclude that the high isobutene selectivity of Pt/H-SAPO-11 (D) and (E) shown in Fig. 5 is caused mainly by the increase in acid strength.

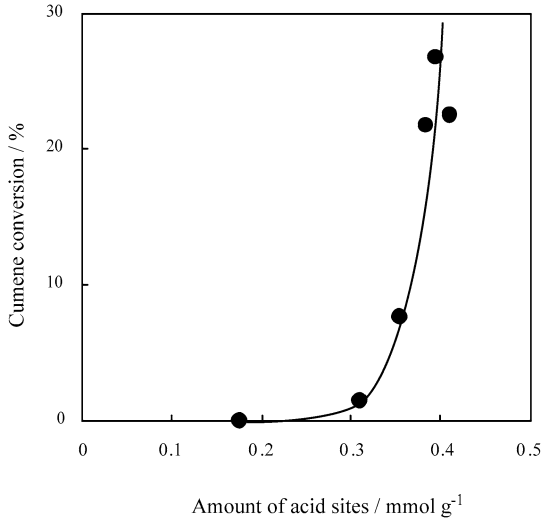

Fig. 7. Effect of the amount of acid sites on the conversion of cumene for H-SAPO-11 with various Si contents.

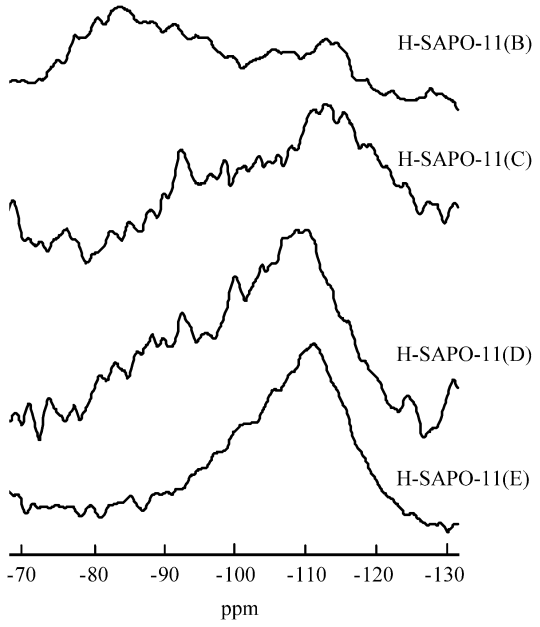

Fig. 8. ^{29}Si MAS NMR spectra of H-SAPO-11 with various Si contents.

3.3. Effect of second elements on catalysis by Pt/H-SAPO-11

To further increase the isobutene selectivity of Pt/H-SAPO-11, we tried to control the hydrogenolysis activity of Pt particles by introducing the second element. Fig. 9 shows the effect of second elements Sn, Pb, Zn, and In on isobutene selectivity compared with that of Pt/H-SAPO-11. Pt and the second element were supported by the co-impregnation method onto H-SAPO-11(D). At lower conversion, the addition of second elements decreased isobutene selectivity, probably because the second elements weakened the isomerization activity of acid sites. At higher conversions, Pt–Sn/H-SAPO-11 gave higher selectivity than Pt/H-SAPO-11 and other modified catalysts. In the case of alkane hydrogenolysis, the similar effect of tin in reducing the hydrogenolysis activity of Pt has been reported [10–13]. We subsequently concentrated on Pt–Sn/H-SAPO-11 to clarify the effect of tin on the selective formation of isobutene. Fig. 10 shows how the amount of tin affects the isobutene selectivity of Pt–Sn/H-SAPO-11(D). Various amounts of tin were supported by the successive impregnation method on Pt/H-SAPO-11. The addition of tin increased the isobutene selectivity at higher conversions, where the selectivity reached 25 C% on Pt–Sn/H-SAPO-11 with Pt/Sn atomic ratios of 0.5, 1.5, and 3.0. A large amount of tin (Pt/Sn = 0.2) further increased the isobutene selectivity but significantly decreased the activity. As shown in Fig. 11, the hydrogenolysis index, α_{hyd}, of all of the Pt–Sn/H-SAPO-11 catalysts was close to 1.0, and was higher for Pt/H-SAPO-11. The hydrogenolysis to form methane

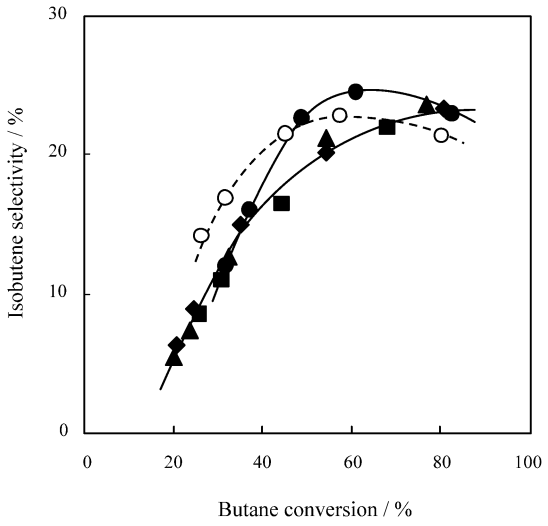

Fig. 9. Isobutene selectivity in the dehydroisomerization of butane on Pt (○), Pt–Sn (●), Pt–Pb (▲), Pt–Zn (◆) and Pt–In (■) supported on H-SAPO-11(D).

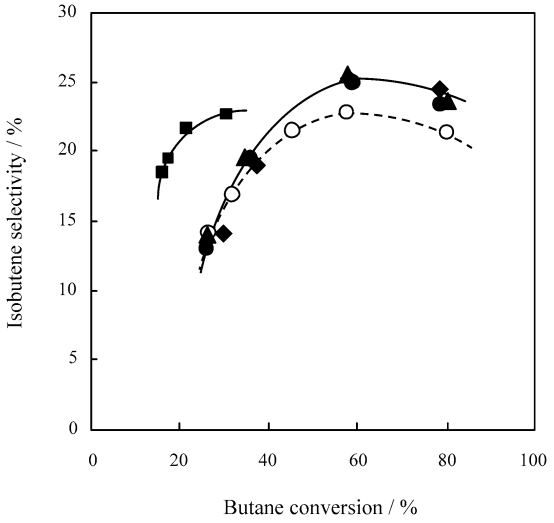

Fig. 10. Isobutene selectivity in the dehydroisomerization of butane on Pt/H-SAPO-11(D) (○) and Pt–Sn/H-SAPO-11(D) with Pt/Sn atomic ratio of 0.2 (■), 0.5 (◆), 1.5 (●) and 3.0 (▲).

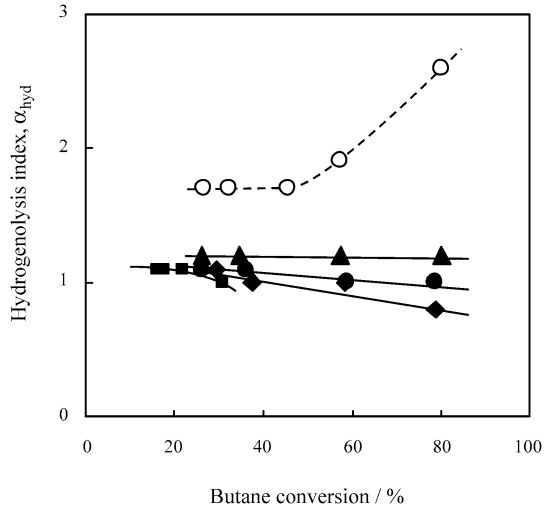

Fig. 11. Hydrogenolysis index of Pt/H-SAPO-11(D) (○) and Pt–Sn/H-SAPO-11(D) with Pt/Sn atomic ratio of 0.2 (■), 0.5 (◆), 1.5 (●) and 3.0 (▲).

on Pt particles was effectively retarded by the addition of tin. Increasing the amount of tin from Pt–Sn(3.0)/H-SAPO-11 to Pt–Sn(0.5)/H-SAPO-11 gradually lowered α_{hyd} at higher conversions, indicating the slight change in the nature of Pt–Sn/H-SAPO-11.

To elucidate the effect of tin on the dehydrogenation activity of Pt, Pt–Sn/H-SAPO-11(D) was used for the catalyst in the dehydrogenation of cyclohexane. Fig. 12 shows the change in cyclohexane conversion with time on steam. Products were mainly benzene, with small amounts of methylcyclopentane, methylcyclopentene, ethane, and propane. The conversion on Pt/H-SAPO-11 decreased rapidly with time on stream. Coke formation occurred on Pt particles. When tin was added in the amount of Pt/Sn = 3.0 and 1.5, the conversion remained constant at ca. 100% for 90 min on stream. Coke formation was retarded by the addition of tin, which is advantageous to dehydrogenation. The further addition of tin lowered the conversion and finally resulted in the almost total loss of activity on Pt–Sn(0.2)/H-SAPO-11. Clearly, addition of the appropriate amount of tin increased the stability of dehydrogenation activity, although in butane dehydroisomerization, the catalytic results were almost the same for Pt–Sn(0.5)/H-SAPO-11 and Pt–Sn(1.5)/H-SAPO-11.

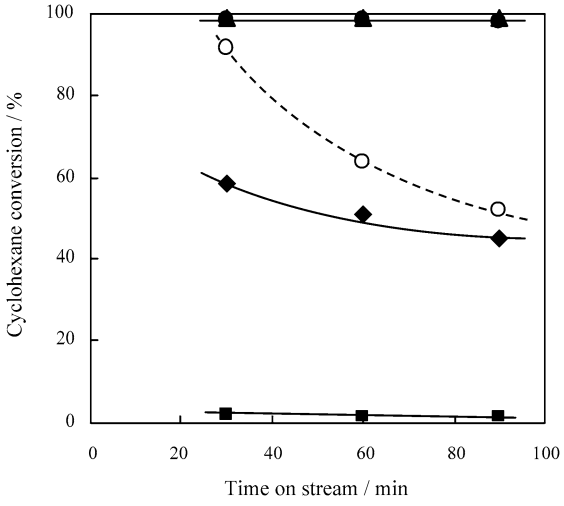

Fig. 12. Dehydrogenation of cyclohexane on Pt/H-SAPO-11(D) (○) and Pt–Sn/H-SAPO-11(D) with Pt/Sn atomic ratio of 0.2 (■), 0.5 (◆), 1.5 (●) and 3.0 (▲).

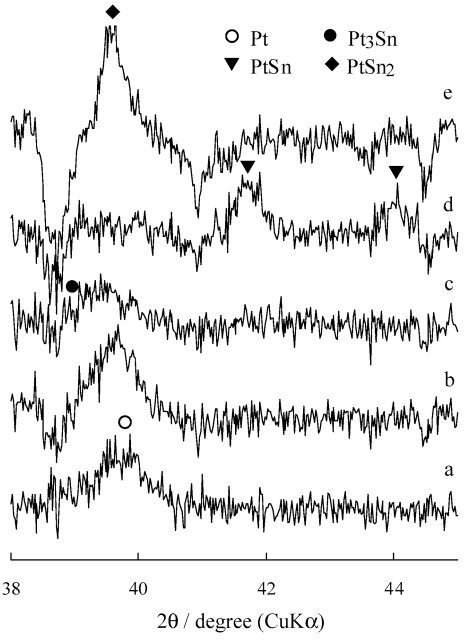

Fig. 13. XRD patterns of Pt/H-SAPO-11(D) (a) and Pt–Sn/H-SAPO-11(D) with Pt/Sn atomic ratio of 3.0 (b), 1.5 (c), 0.5 (d) and 0.2 (e).

3.4. Characterization of Pt–Sn/H-SAPO-11

We now discuss the structural aspect of Pt–Sn metallic particles formed on H-SAPO-11. Fig. 13 shows XRD patterns of Pt–Sn/H-SAPO-11(D) after subtracting the pattern of H-SAPO-11(D) to minimize the influence of the diffraction from the support. Pt/H-SAPO-11 (a) gave a broad peak at around

Table 3
Characterization of metal particles supported on H-SAPO-11

Catalyst	Bulk Pt/Sn[a]	Bulk phase[b]	Crystallite diameter[b] (nm)	Pt dispersion[c] (%)	Surface Pt/Sn[a]
Pt/H-SAPO-11(D)		Pt	8	13	
Pt–Sn(3.0)/H-SAPO-11(D)	3.0	Pt, Alloy	9	7.8	2
Pt–Sn(1.5)/H-SAPO-11(D)	1.5	Alloy, Pt_3Sn	8	6.7	1
Pt–Sn(0.5)/H-SAPO-11(D)	0.5	PtSn	14	2.8	0.6
Pt–Sn(0.2)/H-SAPO-11(D)	0.2	$PtSn_2$	14	0.3	0.04

[a] Atomic ratio.
[b] Obtained from XRD.
[c] Obtained from CO adsorption.

$2\theta = 39.8°$, indicating the presence of Pt particles with crystallite diameter of 8 nm. Pt–Sn(3.0)/H-SAPO-11 (b) gave a broad peak at the similar position to that of Pt metal, although a slight shift to a lower angle could be caused by the formation of Pt-rich alloy (solid solution) with a Pt/Sn ratio >10 [31]. Pt–Sn(1.5)/H-SAPO-11 (c) showed a significant shift of the Pt peak to the lower angle, suggesting formation of the alloy and a slight contribution of an intermetallic compound, Pt_3Sn, whose main diffraction is known to appear at 38.9°. Pt–Sn(0.5)/H-SAPO-11 (d) showed two peaks attributable to an intermetallic compound, PtSn ($2\theta = 41.8°$ and 44.1°). Pt–Sn(0.2)/H-SAPO-11 (e) gave a relatively large peak at 39.9°, which could be assigned to an intermetallic compound, $PtSn_2$ ($2\theta = 39.7°$), although the Pt metal in Pt/H-SAPO-11 (a) gave the peak at almost the same angle. A negative peak at 38.8° indicates the partial destruction of the SAPO-11 structure by the addition of a large amount of tin. The above assignment of XRD peaks are listed in Table 3. The XRD patterns of Pt–Sn/H-SAPO-11 catalysts used for the reaction of butane for 150 min were almost similar to those of the fresh catalysts, indicating that no sintering of metal particles occurred during the reaction.

We obtained the dispersion of Pt from the amount of chemisorbed CO at 298 K on Pt/H-SAPO-11(D) and Pt–Sn/H-SAPO-11(D), as shown in Table 3 with the crystallite diameter of Pt–Sn particles obtained from the peak width in XRD (Fig. 13). In addition, we calculated the surface Pt/Sn atomic ratio by the following procedure. The dispersion is regarded as inversely proportional to the crystallite diameter; therefore, the theoretical Pt dispersion of a pure Pt crystallite with the same diameter as the Pt–Sn crystallite is calculated from the observed dispersion (13.3%) of pure Pt crystallite of 8.2 nm in diameter. The difference between the theoretical and observed dispersions on Pt–Sn/H-SAPO-11 will correspond to the surface Sn atoms, because Sn atoms will not chemisorb CO at 298 K. Then the surface Pt/Sn ratio can be calculated by dividing the theoretical dispersion by the difference in the dispersions mentioned above. Another assumption is the stoichiometry of CO/Pt = 1. The surface Pt/Sn ratios thus obtained are listed in Table 3. Lower surface Pt/Sn ratios compared with corresponding bulk Pt/Sn ratios indicate the surface enrichment in tin. From the XRD results, Pt and Sn easily form an alloy of Pt/Sn > 10 and intermetallic compounds of Pt/Sn = 0.5–3. Pt–Sn particles in Pt–Sn(3.0)/H-SAPO-11 had a surface Pt/Sn ratio of 2, suggesting that the surface may consist of the intermetallic compounds Pt_3Sn and PtSn. In the case of Pt–Sn(1.5)/H-SAPO-11, the surface Pt/Sn ratio of 1 suggests the formation of PtSn on the particle surface. The surface Pt/Sn ratio of Pt–Sn(0.5)/H-SAPO-11 would correspond to the formation of $PtSn_2$, although XRD results showed the presence of bulk PtSn. The very low surface Pt/Sn ratio of Pt–Sn(0.2)/H-SAPO-11 indicates that the surface of $PtSn_2$ particles should be covered by a large amount of tin species. This would be the reason why Pt–Sn(0.2)/H-SAPO-11 gave very low catalytic activity.

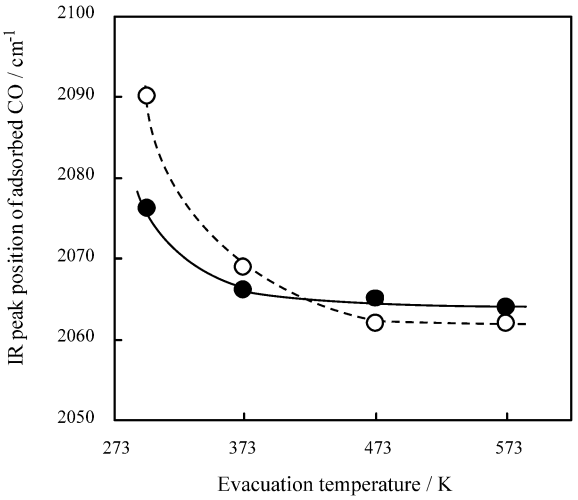

Fig. 14. IR peak position of CO adsorbed on Pt/H-SAPO-11(D) (○) and Pt–Sn (1.5)/H-SAPO-11(D) (●) after the evacuation at each temperature for 10 min.

IR spectra of adsorbed CO were observed to determine the effect of tin on surface Pt atoms. The peak position of adsorbed CO was obtained after evacuation at various temperatures, as shown in Fig. 14. By comparing the peak position of Pt–Sn/H-SAPO-11 with that of Pt/H-SAPO-11 after the high-temperature evacuation, the ligand effect of tin can be elucidated. On the other hand, the difference between the peak positions before and after the high-temperature evacuation indicates the contribution of the ensemble effect of tin [32]. After evacuation at 298 K, the adsorbed CO gave a strong absorption at 2090 cm^{-1} for Pt/H-SAPO-11 and 2076 cm^{-1} for Pt–Sn(1.5)/H-SAPO-11. Evacuation at 573 K shifted the peak position to 2062 and 2064 cm^{-1}, respectively. The similar peak positions for two catalysts after the evacuation at 573 K indicate that the electronic state of Pt on Pt–Sn particles was similar to that on Pt particles; that is, the ligand effect of tin was negligible. On the other hand, the difference in the peak positions before and after the high temperature evacuation was 28 cm^{-1}

for Pt/H-SAPO-11 and 12 cm^{-1} for Pt–Sn(1.5)/H-SAPO-11. The smaller shift in peak position for Pt–Sn catalyst indicates that the distance between adsorbed CO molecules was relatively long before the high-temperature evacuation. This is usually explained as the ensemble effect. Similar ensemble effects have also been reported for Pt–Sn/SiO_2 in the dehydrogenation of isobutane [10] and for Pt–Sn/Na-Y in the dehydrogenation of propane [11]. The ensemble effect found by IR spectra is consistent with formation of the surface Pt–Sn intermetallic compounds discussed above. This intermetallic compound may be formed on the surface of bimetallic particles on Pt–Sn/H-SAPO-11 with Pt/Sn = 0.5–3.0 to effectively retard the hydrogenolysis catalyzed by Pt ensembles.

4. Conclusion

The dehydroisomerization of butane into isobutene is catalyzed by Pt/zeolite catalysts. H-SAPO-11 is the most effective zeolite for the selective formation of isobutene at higher butane conversions. In H-SAPO-11 with higher Si content, the strong acid sites are created inside or around the aluminosilicate region. These acid sites are of appropriate strength to catalyze the isomerization of initially produced 1- and 2-butene into isobutene without accelerating the extensive cracking, oligomerization, and aromatization. The addition of tin onto Pt/H-SAPO-11 with a Pt/Sn atomic ratio of 0.5–3.0 generates particles of Pt-rich alloy and the intermetallic compounds Pt_3Sn and PtSn. The surface of these particles is slightly rich in tin compared with their bulk. The surface formation of intermetallic compounds Pt_3Sn, PtSn, and $PtSn_2$ prevents Pt atoms from forming ensembles active for the hydrogenolysis. As a result, Pt–Sn/H-SAPO-11 with a Pt/Sn ratio of 0.5–3.0 gives high selectivity to isobutene in the dehydroisomerization of butane.

Acknowledgments

We thank Mr. Yukio Takagi and Yoshinori Tanaka for measuring the ^{29}Si MAS NMR spectra and Dr. Hiroyasu Nishiguchi for assisting with the SAPO-11 synthesis.

References

[1] G.D. Pirngruber, K. Seshan, J.A. Lercher, J. Catal. 186 (1999) 188.
[2] G.D. Pirngruber, K. Seshan, J.A. Lercher, J. Catal. 190 (2000) 338.
[3] G.D. Pirngruber, O.P.E. Zinck-Stagno, K. Seshan, J.A. Lercher, J. Catal. 190 (2000) 374.
[4] H. Nagata, Y. Takiyama, S. Tashiro, M. Kishida, K. Wakabayashi, in: M.M.J. Treacy, B.K. Marcus, M.E. Bisher, J.B. Higgins (Eds.), Proc. 12th Int. Zeolite Conference, Baltimore, 5–10 July 1998, MRS, Warrendale, 1999, p. 1141.
[5] G.D. Pirngruber, K. Seshan, J.A. Lercher, J. Catal. 190 (2000) 396.
[6] Y. Wei, G. Wang, Z. Liu, L. Xu, P. Xie, Stud. Surf. Sci. Catal. 154 (2004) 2359.
[7] Y. Wei, G. Wang, Z. Liu, P. Xie, L. Xu, Stud. Surf. Sci. Catal. 142 (2002) 603.
[8] A. Vieira, M.A. Tovar, C. Pfaff, B. Mendez, C.M. Lopez, F.J. Machado, J. Goldwasser, M.M. Ramirez Agudelo, J. Catal. 177 (1998) 60.
[9] A. Vieira, M.A. Tovar, C. Pfaff, P. Betancourt, B. Mendez, C.M. Lopez, F.J. Machado, J. Goldwasser, M.M. Ramirez Agudelo, M. Houalla, J. Mol. Catal. A Chem. 144 (1999) 101.
[10] R.D. Cortright, J.A. Dumesid, J. Catal. 148 (1994) 771.
[11] P. Meriaudeau, A. Thangaraj, J.F. Dutel, C. Naccache, J. Catal. 167 (1997) 180.
[12] S. Miguel, A. Castro, O. Scelza, Catal. Lett. 36 (1996) 201.
[13] O.A. Barias, A. Holmen, E.A. Blekkan, Catal. Today 24 (1995) 361.
[14] P. Meriaudeau, C. Naccache, A. Thangaraj, C.L. Bianchi, R. Carli, V. Vishvanathan, S. Narayanan, J. Catal. 154 (1995) 345.
[15] J. Llorca, N. Homs, J. Leon, J. Sales, J.L.G. Fierro, P. Ramirez de la Piscina, Appl. Catal. A Gen. 189 (1999) 77.
[16] S.B.D.A. Hamid, D. Lambert, E.G. Derouane, Catal. Today 63 (2000) 237.
[17] S. Scirè, G. Burgio, C. Crisafukki, S. Minicò, Appl. Catal. A Gen. 274 (2004) 151.
[18] T. Komatsu, M. Fukui, T. Yashima, in: J.W. Hightower, W.N. Delgass, E. Iglesia, A.T. Bell (Eds.), 11th Int. Congr. Catal., in: Stud. Surf. Sci. Catal., vol. 101, Elseviers Science BV, Amsterdam, 1996, p. 1095.
[19] T. Komatsu, S. Hyodo, T. Yashima, J. Phys. Chem. B 101 (1997) 5565.
[20] A. Onda, T. Komatsu, T. Yashima, Phys. Chem. Chem. Phys. 2 (2000) 2999.
[21] T. Komatsu, D. Satoh, A. Onda, Chem. Commun. (2001) 1080.
[22] A. Onda, T. Komatsu, T. Yashima, J. Catal. 201 (2001) 13.
[23] A. Onda, T. Komatsu, T. Yashima, J. Catal. 221 (2004) 378.
[24] T. Komatsu, Y. Fukui, Appl. Catal. A Gen. 279 (2005) 1730.
[25] T. Komatsu, M. Mesuda, T. Yashima, Appl. Catal. A Gen. 194–195 (2000) 333.
[26] J. Houzvicka, S. Hansildaar, V. Ponec, J. Catal. 167 (1997) 273.
[27] D. Barthomeuf, Zeolites 14 (1994) 394.
[28] M. Martens, J.A. Martens, P.J. Grobet, P.A. Jacobs, in: D. Barthomeuf, E.G. Derouane, W. Hölderich (Eds.), Guideline for Mastering the Properties of Molecular Sieves, NATO ASI Series B221, 1990, p. 1.
[29] T. Masukawa, T. Komatsu, T. Yashima, Zeolites 18 (1997) 10.
[30] P. Meriaudeau, V.A. Tuan, F. Lefebvre, V.T. Ngheim, C. Naccache, Microporous Mesoporous Mater. 22 (1998) 435.
[31] T.B. Massalski, H. Okamoto, P.R. Subramanian, L. Kacprzak (Eds.), Binary Alloy Phase Diagrams, second ed., ASM International, 1990, p. 3132.
[32] M. Primet, J. Catal. 88 (1984) 273.